Electronic Structure Study of the High-pressure Vibrational Spectrum of FeS$_2$ Pyrite

Marc Blanchard,*,† Maria Alfredsson,‡ John Brodholt,‡ G. David Price,‡ Kate Wright,†,§ and C. Richard A. Catlow†

*Royal Institution of Great Britain, 21 Albemarle Street, London W1S 4BS, U.K.*

Received: June 29, 2005; In Final Form: September 16, 2005

Plane-wave density functional calculations are used to investigate the pressure dependence of the geometry and Γ-point phonons of FeS$_2$ pyrite up to 150 GPa. The linear response method is employed to calculate the vibrational properties. Raman-active modes are in excellent agreement with the experimental data available up to 50 GPa,[1] and we predict the evolution with pressure of the IR-active modes for which no high-pressure spectroscopic data have been reported so far. Over the wide pressure range investigated here, all vibrational frequencies depend nonlinearly on pressure; their pressure dependence is quantified by determining the full set of mode Grüneisen parameters and their pressure derivatives.

Introduction

FeS$_2$ pyrite is the most abundant of all metal sulfides and occurs in many different geological environments (sedimentary, magmatic, metamorphic, and hydrothermal deposits). The Fe−S system may also have played an important role in the formation, evolution, and composition of the Earth's core and more generally of the cores in other terrestrial planets (e.g., Venus, Mars).[2] The physical and chemical properties of pyrite have therefore been studied at high temperatures and pressures. Pyrite appears to have a wide stability field according to static compression experiments performed up to 40 GPa[3,4] and shock compression data that suggest that no phase transition should happen up to a pressure of a least 320 GPa.[2] Its equation of state and elastic properties have been determined by using diamond anvil cell equipment up to 50 GPa,[5] which has demonstrated the strong dependence of the equation of state (EOS) on the stress conditions. Electronic properties such as the band gap have also been investigated in order to understand the complex bonding effects induced by the combination of covalent S−S dimers and largely ionic Fe−S bonds.[6] These latter studies are also motivated by the possible application of pyrite as photovoltaic material in solar cells.[7]

Vibrational spectroscopy represents an alternative tool that can be used to investigate a possible structural phase transition and above all to understand the bonding properties. All the phonon frequencies of pyrite have been determined at ambient conditions by IR, Raman spectroscopy, or inelastic neutron scattering experiments.[8−10] These data have been analyzed and modeled by interatomic potential calculations in order to discuss the nature of the atomic bonding.[8,10−12] The most accurate simulations are those using a polarizable-ion model.[13] These simulations were able to reproduce the observed phonon frequencies (i.e., Raman- and IR-active modes) to within an average of better than 3 cm^{-1}. Recently, Kleppe and Jephcoat[1]
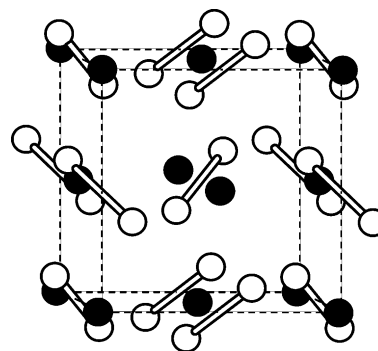
Figure 1. Unit cell of the pyrite structure. Open and filled circles represent S and Fe atoms, respectively.

have investigated the pressure dependence of the phonon frequencies with the acquisition of the Raman spectrum of FeS$_2$ pyrite up to 55 GPa. In this paper, we calculate the vibrational frequencies of pyrite as a function of pressure using the linear response method in the plane-wave density functional approximation. Our study represents the first detailed investigation of the phonon frequencies and their pressure dependence in pyrite by first-principle methods. Thus, these calculations, performed up to 150 GPa, contribute to the understanding of the pressure dependence of the vibrational spectroscopy and thermodynamics, which in turn leads to a better understanding of the Fe−S system in the Earth interior. The pressure range investigated here is limited by the transition to a metallic phase for which the theoretical method no longer applies.

FeS$_2$ pyrite crystallizes in the cubic symmetry (space group *Pa*3 or T_h^6 in Schoenflies notation) with four formula units per unit cell. The Fe^{2+} cations occupy the sites of a face-centered-cubic sublattice, and the (S$_2$)$^{2-}$ dimers are centered at the midpoints of the cube edges and body center, so that in this respect the structure may be considered as NaCl-like (Figure 1). The axes of the (S$_2$)$^{2-}$ dimers are oriented along the [111] directions; each Fe atom is coordinated by six sulfurs in a slightly distorted octahedron and each S atom is bonded to three Fe atoms and its dimer pair. The structure is fully defined by two parameters: the unit cell length, $a_0 = 5.416$ Å and the sulfur fractional coordinate, $u = 0.385$.[14,15] From symmetry considerations alone, it is possible to determine the number of IR-

* To whom correspondence should be addressed. E-mail: marc@ri.ac.uk.
† Royal Institution of Great Britain, 21 Albemarle Street, London W1S 4BS, UK. Tel.: +44 (0)20 7409 2992. Fax: +44 (0)20 7629 3569.
‡ Department of Earth Sciences, University College London, Gower Street, London, WC1E 6BT, U.K.
§ Present address: Nanochemistry Research Institute, Department of Applied Chemistry, Curtin University of Technology, P.O. Box U1987, Perth 6845, Western Australia.

22068 *J. Phys. Chem. B, Vol. 109, No. 46, 2005*

Blanchard et al.
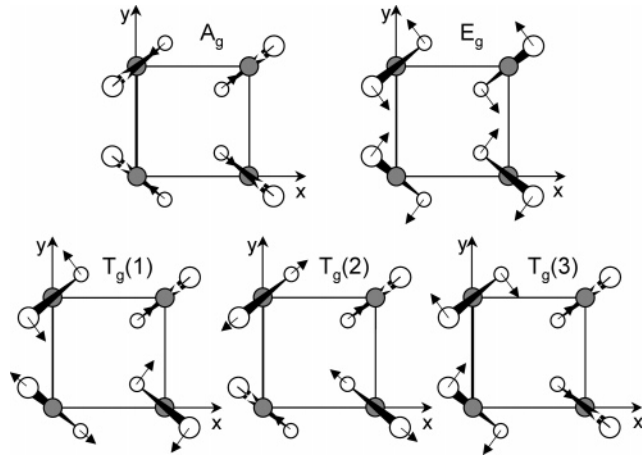
Figure 2. Atomic displacements for the Raman-active modes of FeS$_2$ pyrite (after ref 11). Open and filled circles represent S and Fe atoms, respectively.

and Raman-active modes and, furthermore, to list the symmetry species to which these modes belong. Thus, the 36 dimensional representations of the vibrational matrix for pyrite can be decomposed into the following irreducible representation[12]

$$\Gamma = A_g + E_g + 3T_g + 2A_u + 2E_u + 6T_u$$

The odd-parity species (ungerade) characterize the IR-active (5T$_u$), optically inactive (2A$_u$ + 2E$_u$) modes as well as the rigid lattice translations (T$_u$). On the other hand, the even-parity species (gerade) characterize the Raman-active vibrations (A$_g$ + E$_g$ + 3T$_g$) in which the Fe atoms stay at rest while the sulfur atoms of each dimer move in opposite directions with equal amplitude. The atomic displacements of the five Raman-active modes of pyrite are shown in Figure 2. The totally symmetric A$_g$ mode corresponds to the in-phase stretching vibrations of the (S$_2$)$^{2-}$ dimer. In the doubly degenerate librational E$_g$ mode, the sulfur atoms are displaced perpendicularly to the dimer axis. Finally, the triply degenerate T$_g$ modes can be described by various librational and stretching vibrations or their combinations. A particular case could be out-of-phase stretching vibrations of the (S$_2$)$^{2-}$ dimer, although we should bear in mind that any coupling between librational and stretching motions are allowed by this symmetry species.

The method employed in our first-principle study of the vibrational properties of pyrite is described in the next section. We find good agreement between the calculated and experimental values of the structural and electronic properties. We compare the calculated pressure dependence of the Raman-active frequencies with those measured by Kleppe and Jephcoat[1] and predict the evolution of the IR-active modes as a function of pressure. Finally, the calculated frequencies are used to derive the full set of mode Grüneisen parameters and their pressure derivatives.

Methodology

All the calculations were performed using the CASTEP code,[16] which is based on the implementation of the density functional theory with the electronic density described by a plane-wave basis. Here, we used the norm-conserving pseudo-potentials by Lee.[17] The 3s,3p sulfur orbitals and 3d,4s iron orbitals are treated as valence states. The LDA functional was employed for the determination of the exchange-correlation energy, as parametrized by Perdew and Zunger[18] from the numerical results of Ceperley and Alder.[19] This choice is based

TABLE 1: Measured and Calculated Structural Parameters

| | 0 GPa | | 50 GPa | | 150 GPa |
	exp.[a]	calcd.	exp.[a]	calcd.	calcd.
$a_0{}^b$	5.416	5.380	5.055	5.058	4.756
u^c	0.385	0.385		0.383	0.382
S−S distance[d]	2.162	2.151		2.045	1.937
Fe−S distance[d]		2.248		2.111	1.983

[a] Experimental data are from Merkel et al.,[5] Brostigen and Kjek-shus,[14] and Finklea et al.[15] [b] Cell parameter, a_0, in Å. [c] Sulfur coordinate, u, in fractional unit. [d] S−S and Fe−S Bond Distances in Å.

on the description of the pyrite structure. With norm-conserving pseudopotentials, this exchange-correlation functional gives a 1.2% better value of the cell parameter than the gradient-corrected functional. The size of the plane-wave basis set and the sampling of the Brillouin zone were carefully tested. A Monkhorst−Pack k-point grid[20] of 4 × 4 × 4 was used with which the total energy is within 0.02 meV per atom compared to that calculated for an 8 × 8 × 8 grid. To calculate the phonons, we used an energy cutoff of 550 eV resulting in an error in the phonon frequencies of less than 1 cm^{-1} for all pressures, while the cell parameter is also converged to 1.8 × 10^{-4} Å at zero pressure.

The pyrite structure has been optimized within the *Pa*3 space group and by using the BFGS algorithm,[21] for hydrostatic pressures ranging from 0 to 150 GPa. The total energies are converged to 2.0 × 10^{-5} eV per atom and the forces to 5.0 × 10^{-2} eV/Å. A very small energy tolerance has also been chosen for the electronic minimization (i.e., 1.0 × 10^{-9} eV) in order to achieve a sufficiently well converged set of ground-state wave functions for the subsequent phonon calculations. The density mixing method has been used for the electronic minimization. The phonons were calculated from these optimized geometries by employing the linear response method.[22,23] They were calculated at the Γ-point of the Brillouin zone in order to compare our results with the available Raman and IR spectra, and they include the determination of the longitudinal optical/transverse optical (LO/TO) splitting. The convergence tolerance chosen for the phonon calculations corresponds to a change in the energy derivatives smaller than 3.6 × 10^{-9} eV/Å^2. To verify that the results are independent of the method used, the phonon frequencies and the relative eigenvectors were also calculated with the finite displacement approach at zero pressure. There, the atomic displacement amplitude was tested and finally taken as 5.3 × 10^{-3} Å.

Results and Discussion

Structural and Electronic Properties. The optimized structural parameters of FeS$_2$ pyrite are displayed in Table 1 along with the available experimental measurements. The agreement is very good for the ambient structure as well as the pressure dependence. At zero pressure, the calculated cell parameter is only 0.7% less than the experimental value and becomes nearly equal to that predicted by the EOS of Merkel et al.[5] at 50 GPa. Only a negligible change is observed for the sulfur fractional coordinate, which induces a difference of 0.5% for the S−S bond distance. This result is important since to a first approximation the vibrational frequencies are dependent on bond distances. As expected experimentally and theoretically,[4,24,25] the Fe−S and S−S bond lengths decrease with pressure (Figure 3). We can also note that the Fe−S bonds shorten slightly faster than the S−S bonds, which disagrees with the atomistic simulation results of Sithole et al.[25]
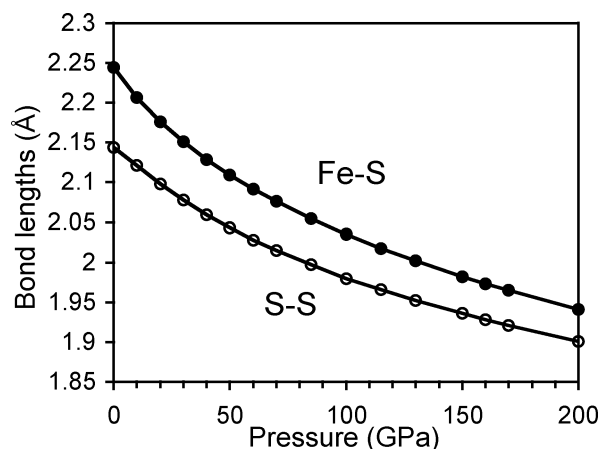
High-Pressure Vibrational Spectrum of Pyrite

J. Phys. Chem. B, Vol. 109, No. 46, 2005 **22069**

Figure 3. Calculated bond lengths as a function of pressure.
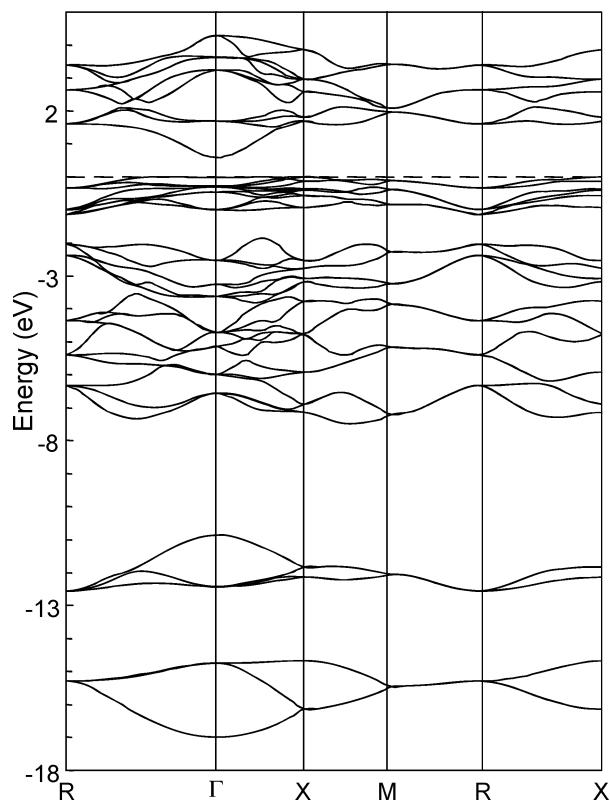
Figure 4. Band structure of pyrite calculated at 0 GPa.

Figure 5. Partial densities of states of pyrite calculated at 0 GPa for the iron d orbitals and sulfur p orbitals compared to the total density of state.
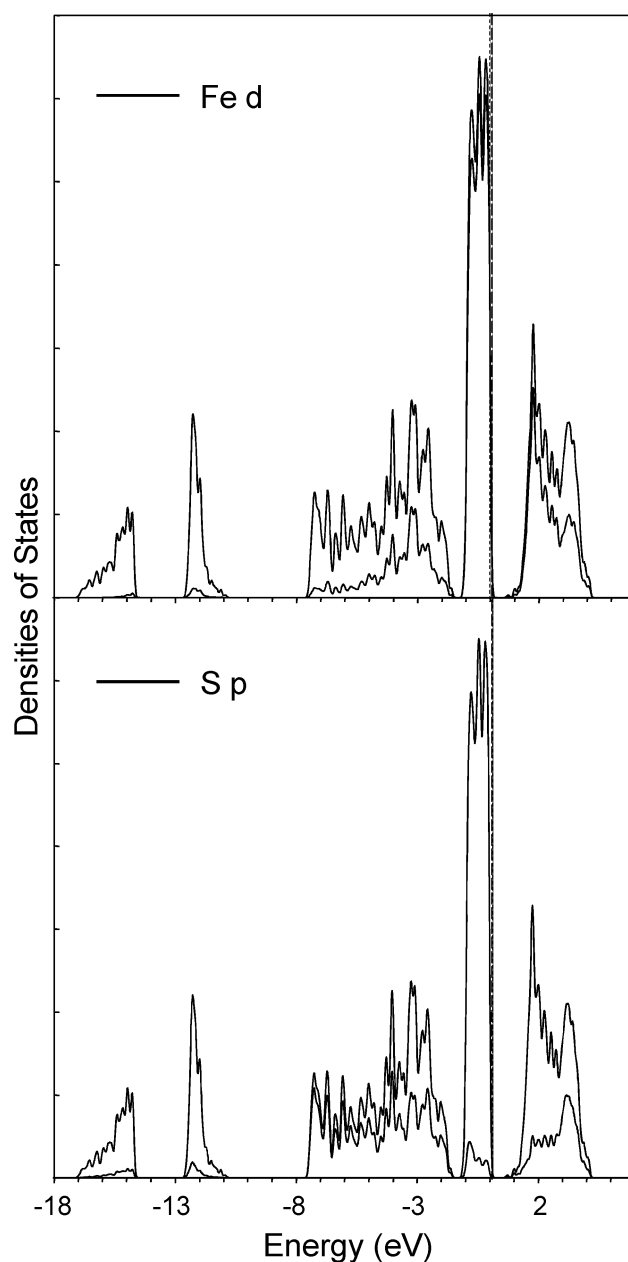
Experimentally, FeS_2 pyrite is diamagnetic and, therefore, the six 3d electrons of Fe^{2+} fill the t_{2g} orbitals leaving the e_g orbitals empty.[26] We performed calculations on the diamagnetic, ferromagnetic, and two antiferromagnetic structures of FeS_2 at zero pressure, and the diamagnetic structure is indeed found to be the most stable, which confirms the low-spin state of the iron ions. The band structure and partial densities of states calculated at 0 GPa are displayed in Figures 4 and 5. Our calculations show an excellent agreement with those of Eyert et al.[27] who made a detailed description and interpretation of the electronic structure. We observe, in Figure 4, a band gap of about 0.6 eV. Closer inspection shows that the band gap is indirect with the valence band maximum located near the X-point in the first Brillouin zone and the conduction band minimum at the Γ-point. Indeed, pyrite is known for its semiconducting properties,[28] and the experimental studies of optical and conductivity measurements indicate an indirect band gap of about 0.9 eV.[6,29] The calculated partial densities of states help us to understand the electronic character of the band gap (Figure 5). We find that

the valence band, and more especially its highest lying bands, is mainly composed of iron 3d t_{2g}-derived states, while the conduction band is described by hybridized iron 3d and sulfur 3p states. The iron contribution is strong, but at the exact conduction band minimum, only a contribution from the sulfur 3p states is observed, which has been shown by other recent theoretical studies.[27,30] Furthermore, the band structures calculated at higher pressures (not presented here) display the same features as at zero pressure but with a progressive dispersion of all bands, which leads to a continuous decrease of the band gap, which remains indirect. The evolution of the calculated band gap energy is plotted in Figure 6 as a function of pressure including the experimental trend observed by Cervantes et al.[6] On the basis of the observation that the LDA functional slightly underestimates the volume of the unit cell, the theoretical pressures were re-estimated from the calculated volume by using the third-order Birch Murnaghan EOS determined by Merkel et al.[5] The fact that the size of the band gap decreases with

22070 *J. Phys. Chem. B, Vol. 109, No. 46, 2005*

Blanchard et al.
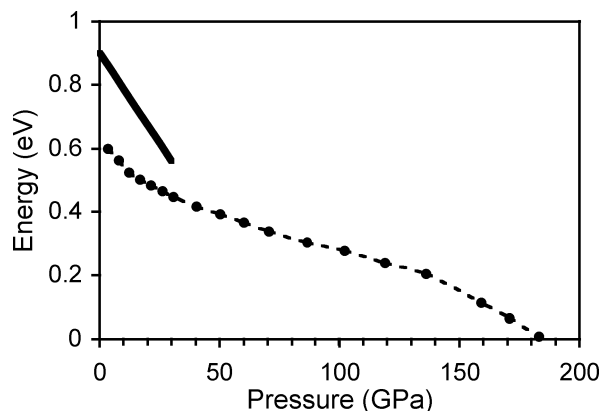
Figure 6. Band gap energy of pyrite as a function of pressure. The points highlighted by the dashed line are the calculated values while the bold line corresponds to the fit of the experimental data obtained by Cervantes et al.[6]

TABLE 2: Measured and Calculated Phonon Frequencies at 0 GPa (in cm^{-1})

		exp.[10]	calcd.			exp.[10]	calcd.
T_u	s^a	0	0	$T_u(3)$ LO	ir	350	365
$T_u(1)$ TO	ir^a	230	221	$T_g(1)$	R	351	366
$T_u(1)$ LO	ir	230	221	A_g	R	381	391
$A_u(1)$	s	211	222	$T_u(4)$ TO	ir	401	392
$E_u(1)$	s	211	246	$T_u(4)$ LO	ir	411	392
$T_u(2)$ TO	ir	293	317	$T_g(2)$	R	378	400
$T_u(2)$ LO	ir	294	320	$E_u(2)$	s	n.a.	404
$A_u(2)$	s	n.a.	343	$T_u(5)$ TO	ir	412	428
E_g	R^a	346	360	$T_g(3)$	R	433	446
$T_u(3)$ TO	ir	348	361	$T_u(5)$ LO	ir	439	480

^{a} s, ir, and R refer to silent, IR-active, and Raman-active modes, respectively.

pressure, as observed from experiments, is consistent with the contraction of the Fe−S and S−S bonds. Moreover, Cervantes et al.[6] have extrapolated linearly their optical spectroscopy data to predict that pyrite will become a metal beyond a pressure of about 80 GPa. The quantitative results of our theoretical study must be considered carefully since it is known that LDA, being a ground-state theory, does not describe properly band gap properties. However, if we look at the pressure dependence of the gap, then we note that its decrease is continuous but not linear with pressure being steeper at lower pressure. This observation suggests that iron pyrite may stay a semiconductor up to pressures higher than 80 GPa. The calculations here predict that the metallization of FeS_2 pyrite will occur at about 180 GPa. However it is difficult to predict an exact pressure for the insulator−metal transition since our LDA calculations underestimate the band gap.

Raman-Active Modes. The Γ-point vibrational frequencies and eigenvectors are calculated for each pressure at the equilibrium geometries. Table 2 displays a general comparison of all the phonon frequencies calculated at zero pressure with experimental measurements obtained by inelastic neutron scattering. These modes are either IR-active or Raman-active or silent. We now discuss in detail the optical modes starting by considering the Raman-active modes for which high-pressure experimental data are available.

The frequencies calculated at zero pressure are reported in Table 3 along with the experimental values measured at ambient conditions. All the calculated frequencies are slightly higher than the observed values. The best agreement is found for the A_g mode with a difference of ca. 12 cm^{-1}. The E_g, $T_g(1)$, and $T_g(3)$ modes are upshifted by about 16 cm^{-1}, and the $T_g(2)$ mode

TABLE 3: Measured and Calculated Raman-Active Frequencies at 0 GPa (in cm^{-1})

| mode	exp.[9]	exp.[1]	linear response	finite displacement
E_g	343	344	360	360
$T_g(1)$	350	350	366	366
$T_g(2)$	377		400	400
A_g	379	379	391	391
$T_g(3)$	430	430	446	446

displays the largest difference with 23 cm^{-1}, corresponding to errors of 3−6%. These small discrepancies are mainly due to the difference observed between the calculated and the experimental volume. For the same volume, the frequencies differ by less than 5 cm^{-1} for all the modes except the $T_g(2)$ mode, which differs by 10 cm^{-1} (i.e., errors of 1−3%). The agreement between the experimental and calculated Raman-active frequencies at zero pressure is thus very good.

The only significant discrepancy between the calculations and experiment concerns the $T_g(2)$ mode, which shows a change in the relative order compared to the A_g mode, since the frequency of the $T_g(2)$ mode becomes higher than that of the A_g mode. In the literature, the former mode is often interpreted as the out-of-phase stretching vibrations of the S_2 bonds (Figure 2). However, in our calculations, this mode does not correspond to the pure stretching motion but instead to coupled librational and stretching motions of the S_2 dimers. This result can be explained by applying the concept of Davydov splitting, which assumes the stretching of the S_2 dimer to be split into A_g and T_g components when the S_2 molecules occupy their four equivalent sites in the $Pa3$ structure. Likewise the doubly degenerate rotation of the S_2 dimers can be converted into three librational modes with symmetry $E_g + 2T_g$. However, as mentioned previously, there is no clear separation between the stretching and librational modes. The coupling may be considered small if the separation between the E_g and A_g frequencies is substantial. In the case of FeS_2, we calculate a small difference of 31 cm^{-1} at zero pressure; the experimental observation by Vogt et al.[9] is about 36 cm^{-1}. We can therefore assume that there is a substantial coupling between the librational and stretching modes of the S_2 dimers in FeS_2. In contrast, in MnS_2 pyrite, the corresponding splitting between the E_g and A_g modes is reported to be ca. 240 cm^{-1}.[9] In this case, where no coupling between stretching and librations should occur, the T_g bands are shifted to lower values compared to the E_g and A_g modes.

To check the reliability of these results and to investigate if the small discrepancies between calculated and experimental data are caused by the method employed, the phonon frequencies and associated eigenvectors were also calculated at 0 GPa by using the finite displacement method. We find an excellent agreement between the two methods (Table 3) and still have the same change of the relative order between the $T_g(2)$ and the A_g modes. The eigenvectors also exhibit the same features for both methods. The only difference would deal with the contribution of stretching motions of the T_g modes, which seems to be stronger with the linear response than with the finite displacement method.

The Raman-active frequencies calculated using the linear response method are reported as a function of pressure in Table 4. The corrected pressures (see previous section) that have been used to plot Figure 7 are also listed. The calculated A_g and $T_g(3)$ modes are in excellent agreement with the experimental data of Kleppe and Jephcoat,[1] while the E_g and $T_g(1)$ modes show a blue shift of 5−10 cm^{-1} in agreement with zero pressure data (Figure 7). The $T_g(2)$ mode could not be resolved in the experimental unpolarized spectra because of its low intensity

High-Pressure Vibrational Spectrum of Pyrite

J. Phys. Chem. B, Vol. 109, No. 46, 2005 **22071**
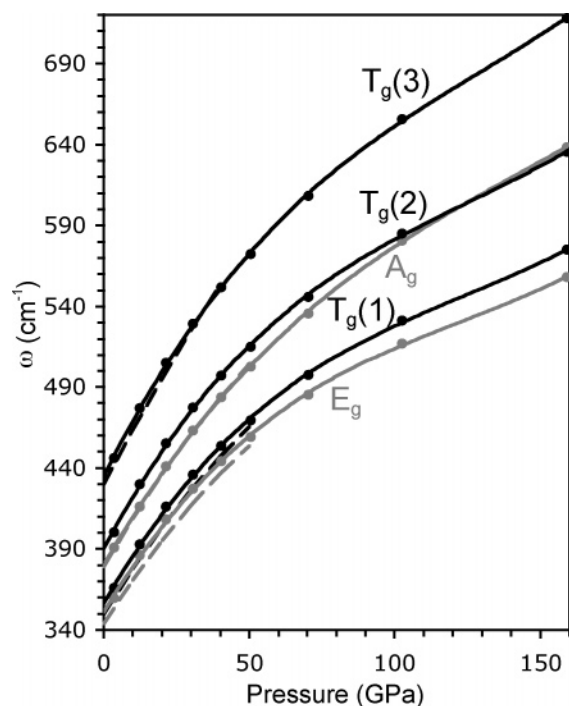
Figure 7. Evolution of the Raman-active modes with pressure. The points are the calculated frequencies plotted vs corrected pressures and fitted by a third-order polynomial. Bold dashed lines are experimental data from Kleppe and Jephcoat.[1]

TABLE 4: Calculated Raman-Active Frequencies (in cm^{-1}) as a Function of Pressure

P^a	P cor.^{b}	E_g	$T_g(1)$	A_g	$T_g(2)$	$T_g(3)$
0	3.6	360	366	391	401	446
10	12.3	386	393	416	430	477
20	21.4	408	416	441	455	505
30	30.7	427	436	463	477	530
40	40.3	444	454	484	497	552
50	50.3	459	470	503	515	572
70	70.4	485	497	536	546	608
100	102.5	517	531	581	585	656
150	159.1	558	575	639	636	718

^{a} P represents the input hydrostatic pressure (in GPa). ^{b} P cor., the corrected pressure (in GPa).

and because it stays relatively close to the Ag mode, which has the highest intensity.[1] On the basis of the zero pressure data, we assume that the calculated $T_g(2)$ mode is upshifted by 10–15 cm^{-1}. The evolution of the Raman-active frequencies as a function of pressure is well reproduced in our calculations compared to experiments. We observe a continuous increase of all Raman frequencies up to the highest pressure investigated here, which is due to the progressive pressure-induced contraction of the S–S and Fe–S bonds.

All modes tend to separate with pressure; only the A_g mode shows a different behavior. The curvature of the A_g mode is smaller than that of the $T_g(2)$ mode (see Table 7), which results in a crossover in frequency between the two modes at about 125 GPa. This in-phase stretching mode only involves the S–S bond whereas all other modes that have at least a contribution from librational motion are largely controlled by the strength of the Fe–S bond. This difference can explain the special pressure dependence of the A_g mode, along with the prediction from our simulations of a slower shortening with pressure of the S–S bonds compared with the Fe–S bonds. The crossover between the A_g and $T_g(2)$ modes may not occur in nature since the $T_g(2)$ mode is observed at 2 cm^{-1} below the A_g mode in ambient spectra.[9]

IR-Active Modes. The IR-active frequencies calculated as a function of pressure are given in Table 5, and Figure 8 shows their evolution once the pressure has been corrected following the same procedure as before. Figure 8 also shows the experimental IR frequencies acquired at zero pressure by IR spectroscopy or inelastic neutron scattering.[10,31] The calculated frequencies extrapolated at 0 GPa fall at 5–30 cm^{-1} around the experimental values (i.e., error of 1–10%). This discrepancy, although acceptable, is larger than that obtained for the Raman-active modes. No high-pressure IR spectra are available for pyrite, but the good agreement obtained for the pressure dependence of the Raman modes allows us to consider the evolution of the IR frequencies with a high confidence.

As with the Raman-active modes, all the IR frequencies increase up to the pressure of about 180 GPa where pyrite becomes a metal in our simulation. Therefore, there is no indication of a structural phase transition associated with this metallization, which is in agreement with the shock compression data.[2] Moreover, within this general trend, two distinct behaviors can be distinguished: the $T_u(1)$ and $T_u(3)$ modes show a small pressure dependence with approximately the same curvature, while the frequencies of the three other modes strongly increased with pressure, with a larger curvature (see Table 8), one reason for which can be found from a close inspection of the eigenvectors. All IR-active modes involve Fe–S stretching and bending vibrations while S–S dimers only undergo translations. Thus, in contrast to the Raman-active modes, the S–S bonding influences very little the frequencies of the IR-active modes. The difference of behavior originates from the contribution of the Fe–S stretching motion, which is negligible for the $T_u(1)$ and $T_u(3)$ modes. Thus, the effect of pressure on the lattice vibration of these two modes is limited compared to the other modes.

The use of the linear response method has enabled us to calculate the LO/TO splittings, which are related to the coupling of the atomic displacements with the long-range electric field and as such depend on the charges and polarizability of the

TABLE 5: Experimental[10] and Calculated IR-Active Frequencies (in cm^{-1}) as a Function of Pressure

P^a	P cor.^{b}	$T_u(1)$ TO^c	$T_u(1)$ LO^c	$T_u(2)$ TO	$T_u(2)$ LO	$T_u(3)$ TO	$T_u(3)$ LO	$T_u(4)$ TO	$T_u(4)$ LO	$T_u(5)$ TO	$T_u(5)$ LO
0 (ref 10)		230	230	293	294	348	350	401	411	412	439
0	3.6	221	221	317	320	361	365	392	392	428	480
10	12.3	231	232	346	349	375	380	433	434	463	519
20	21.4	239	239	370	374	386	392	468	469	494	553
30	30.7	245	245	389	393	396	403	497	498	518	581
40	40.3	250	250	409	416	401	407	524	524	541	607
50	50.3	254	255	424	431	409	416	547	547	561	630
70	70.4	260	262	451	459	420	429	587	588	597	670
100	102.5	266	269	484	493	434	444	635	637	642	719
150	159.1	272	277	527	538	451	463	691	701	706	782

^{a} P represents the input hydrostatic pressure (in GPa). ^{b} P cor., the corrected one (in GPa). ^{c} TO and LO correspond to transverse and longitudinal optical modes, respectively.

TABLE 6: Born Effective Charges of the Atoms S (u,u,u) and Fe (0,0,0) as a Function of Pressure

	0 GPa			50 GPa			100 GPa		
S	2.357	0.003	0.148	2.753	−0.054	0.120	2.952	−0.075	0.115
	0.148	2.357	0.003	0.120	2.753	−0.054	0.115	2.952	−0.075
	0.003	0.148	2.357	−0.054	0.120	2.753	−0.075	0.115	2.952
Fe	−4.715	−0.142	−0.354	−5.505	−0.110	−0.296	−5.905	−0.115	−0.250
	−0.354	−4.715	−0.142	−0.296	−5.505	−0.110	−0.250	−5.905	−0.115
	−0.142	−0.354	−4.715	−0.110	−0.296	−5.505	−0.115	−0.250	−5.905

TABLE 7: Extrapolated Zero-Pressure Frequencies and Mode Grüneisen Parameters (γ_{i0}) and Their Pressure Derivatives (q_{i0}) for the Raman-active Modes of Pyrite[a]

modes	freq. (cm^{-1})	γ_{i0} (ref 1)	γ_{i0} (0−50 GPa)	γ_{i0} (100−150 GPa)	γ_{i0} (0−150 GPa)	$\partial^2 \nu_i / \partial P^2$ (cm^{-1}·GPa^{2-})	q_{i0}
E_g	351	1.36	1.33	0.99	1.20	−0.018	−2.10
$T_g(1)$	357	1.39	1.37	1.02	1.24	−0.019	−2.10
A_g	380	1.40	1.39	1.22	1.36	−0.015	−2.41
$T_g(2)$	390		1.38	1.06	1.26	−0.020	−2.14
$T_g(3)$	435	1.42	1.36	1.17	1.30	−0.019	−2.30

a See explanations in text.

TABLE 8: Extrapolated Zero-Pressure Frequencies and Mode Grüneisen Parameters (γ_{i0}) and Their Pressure Derivatives (q_{i0}) for the IR-Active Modes of Pyrite[a]

modes	freq. (cm^{-1})	γ_{i0} (0−50 GPa)	γ_{i0} (100−150 GPa)	γ_{i0} (0−150 GPa)	$\partial^2 \nu_i / \partial P^2$ (cm^{-1}·GPa^{2-})	q_{i0}
$T_u(1)$ TO	219	0.74	0.34	0.56	−0.009	−1.91
$T_u(1)$ LO	219	0.77	0.42	0.61	−0.008	−2.08
$T_u(2)$ TO	308	1.58	1.15	1.38	−0.021	−1.77
$T_u(2)$ LO	310	1.63	1.17	1.42	−0.022	−1.70
$T_u(3)$ TO	357	0.67	0.52	0.61	−0.010	−2.60
$T_u(3)$ LO	362	0.70	0.57	0.64	−0.010	−2.61
$T_u(4)$ TO	378	1.82	1.18	1.55	−0.029	−1.56
$T_u(4)$ LO	379	1.82	1.29	1.58	−0.029	−1.56
$T_u(5)$ TO	417	1.48	1.23	1.35	−0.025	−1.93
$T_u(5)$ LO	467	1.49	1.14	1.33	−0.027	−1.95

a See explanations in text.

ions. The LO/TO splitting can, thus, give important information of the atomic interactions in the material; experimental data were reported by Bührer et al.[10] and Lutz et al.[31] In agreement with the experimental studies, we observe the largest LO/TO splitting
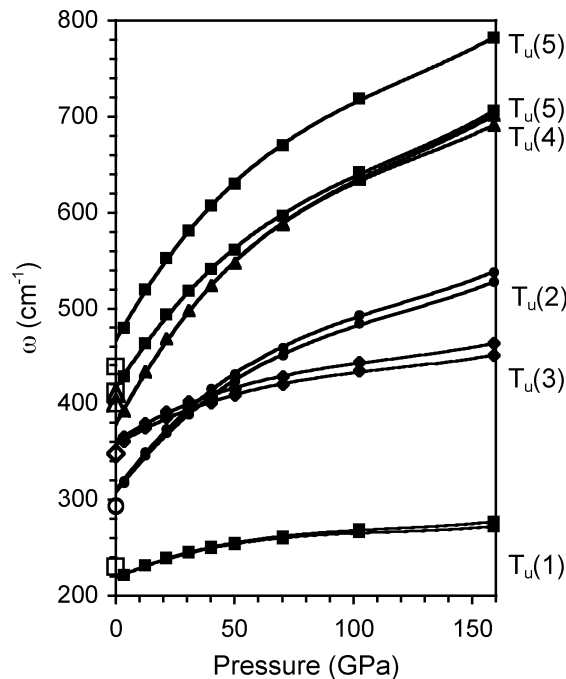
Figure 8. Evolution of the IR-active modes with pressure. The points are the calculated frequencies plotted vs corrected pressures and fitted by a third-order polynomial. The open symbols at 0 GPa are experimental data from Bührer et al.[10] and Lutz et al.[31]

for the $T_u(5)$ mode. However, while the experimental value for the LO/TO splitting is 27 cm^{-1},[10,31] the calculated value is 52 cm^{-1}. The LO/TO splittings can be analyzed by means of the Born effective charges since they describe the coupling between the atomic displacements and the long-range electric field. Our calculated Born effective charge tensors for the S atom of coordinate (u,u,u) and the Fe atom of coordinate (0,0,0) as a function of pressure are given in Table 6. The tensors of the other atomic positions can be obtained by using the symmetry operations of the crystal. These tensors display a small but significant anisotropy, which expresses the deviation from ionicity in the bondings. As the pressure increases so does the trace of the tensors while the nondiagonal components decrease. The LO/TO splitting also depends on the dielectric permittivity. Thus, the observed decrease of the dielectric permittivity as a function of pressure contributes to the increase of the LO/TO splitting but only to a small extent. We can then conclude that it is the increasing diagonal Born effective charges, which contributes the most to the increasing LO/TO splittings as a function of pressure.

Mode Grüneisen Parameters. All the previous observations can be specified by determining quantitatively the pressure dependence of each vibrational mode, that is, the mode Grüneisen parameters. These parameters are of great interest in geophysics since they are used to constrain the pressure and temperature dependence of material thermal properties. Unfortunately, the full set of mode Grüneisen parameters is very difficult to determine experimentally. In FeS$_2$ pyrite, Kleppe and Jephcoat[1] have determined these parameters for the four Raman-active modes they were able to distinguish. However, we can note from our calculations a greater curvature of the

High-Pressure Vibrational Spectrum of Pyrite

J. Phys. Chem. B, Vol. 109, No. 46, 2005 **22073**

frequencies as a function of pressure (Figure 7). Therefore, the extrapolation of the experimental data beyond the 50 GPa investigated by Kleppe and Jephcoat[1] would diverge significantly from our simulations. The mode Grüneisen parameter corresponds to the volume dependence of the ith vibrational mode of the lattice and can be written as follows

$$\gamma_{i0} = - \left. \frac{\partial(\ln \omega_i)}{\partial(\ln V)} \right|_0$$

where ω_i is the frequency of the ith vibrational mode and V, the volume of the unit cell. Then, γ_{i0} was obtained from fitting linearly the variation of $\ln \omega_i$ with $\ln V$ values. Because of the nonlinear pressure dependence of the frequencies, this parameter is not constant over the full pressure range. To compare with experimental data, we first consider the range 0–50 GPa where the pressure dependence can be approximated as linear. This yields values in good agreement with those of Kleppe and Jephcoat[1] (Table 7). They gradually decrease with the pressure, and the value over the full range, 0–150 GPa, is only a rough average (Tables 7 and 8). It is therefore necessary to introduce the pressure derivatives of the mode Grüneisen parameters, which are defined as follows[32]

$$q_{i0} = \gamma_{i0} - K'_0 - \frac{K_0{}^2}{\omega_{i0}\gamma_{i0}} \left. \frac{\partial^2 \omega_i}{\partial P^2} \right|_0$$

where K and K' are, respectively, the bulk modulus and its pressure derivative. They were calculated by fitting the third-order Birch–Murnaghan EOS to the calculated values of energy vs the unit cell volume ($K = 176.21$ GPa and $K' = 4.65$). While the frequency at zero pressure (ω_{i0}) and the frequencies curvature ($\partial^2\omega_i/\partial P^2$) have been obtained from a third-order polynomial fit (Tables 7 and 8).

It is usual to calculate the average of all the mode Grüneisen parameters in order to get an approximate value of the thermal Grüneisen parameter. Thus, we obtain an average of about 1.30 for the first 50 GPa and 1.16 for the full pressure range. These values are lower than that estimated by Ahrens and Jeanloz[2] for FeS_2 pyrite, that is, 1.56 ± 0.16. This observation is, however, in accord with the general trend highlighted by Hofmeister and Mao,[32] which shows that the thermal Grüneisen parameter is often in practice underestimated by the average of the mode Grüneisen parameters. This discrepancy is caused by several factors: the sum should rigorously include both optic and acoustic modes and be averaged over the Brillouin zone; but this point could not explain by itself the discrepancy observed. Hofmeister and Mao[32] have demonstrated that the main reason comes from the general equation used here to obtain the γ_{i0}, which applies to monatomic and diatomic solids but for more complex structures with more than one relevant interatomic distance, we should consider the volume that changes during the particular atomic motion correlated with each given frequency. Unfortunately, this approach cannot be applied directly to the FeS_2 pyrite structure.

Summary and Conclusions

The Γ-point phonon properties of FeS_2 pyrite have been computed up to a hydrostatic pressure of 150 GPa using the linear response method. The structural and electronic parameters are in good agreement with the experimental data. However, the pressure-induced decrease of the band gap suggests that pyrite will become a metal at a much higher pressure than the extrapolated experimental value of 80 GPa.[6] The calculated

Raman-active frequencies are in accord with those measured up to 50 GPa by Kleppe and Jephcoat[1] while high-pressure infrared spectroscopy should be undertaken in order to confirm the frequencies evolution predicted by this study. The A_g Raman mode displays an individual pressure dependence caused by the involvement only of S–S stretching vibrations; while the $T_g(2)$ mode demonstrates a coupling between the stretching and libration, proposed to be caused by the small difference in frequency of the A_g and E_g modes. In infrared modes, two distinct types of pressure dependence are shown depending on the contribution of Fe–S stretching motions. But for all vibrational modes, the frequencies increase continuously with pressure, which confirms the structural stability of pyrite even close to its metallization. The wide pressure range probed here which would be difficult to investigate experimentally, shows a nonlinear pressure dependence of the vibrational frequencies. This curvature must be taken into account for an extrapolation of the vibrational properties at highest pressures. Therefore a full set of mode Grüneisen parameters and their pressure derivatives have been derived.

References and Notes

(1) Kleppe, A. K.; Jephcoat, A. P. *Mineral. Magn.* **2004**, *68*, 433.
(2) Ahrens, T. J.; Jeanloz, R. *J. Geophys. Res.* **1987**, *92*, 10363.
(3) Chattopadhyay, T.; von Schnering, H. G. *J. Phys. Chem. Solids* **1985**, *46*, 113.
(4) Fujii, T.; Yoshida, A.; Tanaka, K.; Marumo, F.; Nodo, Y. *Mineral. J.* **1986**, *13*, 202.
(5) Merkel, S.; Jephcoat, A. P.; Shu, J.; Mao, H.-K.; Gillet, P.; Hemley, R. J. *Phys. Chem. Miner.* **2002**, *29*, 1.
(6) Cervantes, P.; Slanic, Z.; Bridges, F.; Knittle, E.; Williams, Q. *J. Phys. Chem. Solids* **2002**, *63*, 1927.
(7) Ferrer, I. J.; Sánchez, C. *Solid State Commun.* **1992**, *81*, 371.
(8) Verble, J. L.; Wallis, R. F. *Phys. Rev.* **1969**, *182*, 783.
(9) Vogt, H.; Chattopadhyay, T.; Stolz, H. J. *J. Phys. Chem. Solids* **1983**, *44*, 869.
(10) Bührer, W.; Lafougère, E.; Lutz, H. *J. Phys. Chem. Solids* **1993**, *54*, 1557.
(11) Sourisseau, C.; Cavagnat, R.; Fouassier, M. *J. Phys. Chem. Solids* **1991**, *52*, 537.
(12) Lutz, H. D.; Willich, P. *Z. Anorg. Allg. Chem.* **1974**, *405*, 176.
(13) Lutz, H. D.; Zwinscher, J. *Phys. Chem. Miner.* **1996**, *23*, 497.
(14) Brostigen, G.; Kjekshus, A. *Acta Chem. Scand.* **1969**, *23*, 2186.
(15) Finklea, S. L.; Cathey, L.; Amma, E. L. *Acta Crystallogr. A* **1976**, *32*, 529.
(16) Segall, M. D.; Lindan, P. L. D.; Probert, M. J.; Pickard, C. J.; Hasnip, P. J.; Clark, S. J.; Payne, M. C. *J. Phys.: Condens. Matter* **2002**, *14*, 2717.
(17) Lee, M. H. Ph.D. Thesis, Cambridge University, 1996.
(18) Perdew, J. P.; Zunger, A. *Phys. Rev. B* **1981**, *23*, 5048.
(19) Ceperley, D. M.; Alder, B. J. *Phys. Rev. Lett.* **1980**, *45*, 566.
(20) Monkhorst, H. J.; Pack, J. D. *Phys. Rev. B* **1976**, *13*, 5188.
(21) Fischer, T. H.; Almlof, J. *J. Phys. Chem.* **1992**, 96, 9768.
(22) Gonze, X. *Phys. Rev. B* **1997**, *55*, 10337.
(23) Gonze, X.; Lee, C. *Phys. Rev. B* **1997**, *55*, 10355.
(24) Sithole, H. M.; Nguyen-Manh, D.; Pettifor, D. G.; Ngoepe, P. E. *Mol. Simul.* **1999**, *22*, 31.
(25) Sithole, H. M.; Ngoepe, P. E.; Wright, K. *Phys. Chem. Miner.* **2003**, *30*, 615.
(26) Miyahara, S.; Teranishi, T. *J. Appl. Phys.* **1968**, *39*, 896.
(27) Eyert, V.; Höck, K.-H.; Fiechter, S.; Tributsh, H. *Phys. Rev. B* **1998**, *57*, 6350.
(28) Bither, T. A.; Bouchard, R. J.; Cloud, W. H.; Donohue, P. C.; Siemons, W. J. *Inorg. Chem.* **1968**, *7*, 2208.
(29) Schlegel, A.; Wachter, P. *J. Phys. C: Solid State Phys.* **1976**, *9*, 3363.
(30) Muscat, J.; Hung, A.; Russo, S.; Yarovsky, I. *Phys. Rev. B* **2002**, *65*, 054107.
(31) Lutz, H. D.; Schneider, G.; Kliche, G. *J. Phys. Chem. Solids* **1985**, *46*, 437.
(32) Hofmeister, A. M.; Mao, H. *Proc. Natl. Acad. Sci.* **2002**, *99*, 559.